Bioorganic & Medicinal Chemistry Letters 26 (2016) 1675–1679

Contents lists available at ScienceDirect

Bioorganic & Medicinal Chemistry Letters

journal homepage: www.elsevier.com/locate/bmcl

Synthesis and evaluation of ^{18}F-trifluoroborate derivatives of triphenylphosphonium for myocardial perfusion imaging

Zhengxing Zhang [a], Silvia Jenni [a], Chengcheng Zhang [a], Helen Merkens [a], Joseph Lau [a], Zhibo Liu [b], David M. Perrin [b], François Bénard [a,c,*,†], Kuo-Shyan Lin [a,c,*,‡]

[a] Department of Molecular Oncology, BC Cancer Agency, Vancouver, BC V5Z 1L3, Canada
[b] Department of Chemistry, University of British Columbia, Vancouver, BC V6T 1Z1, Canada
[c] Department of Radiology, University of British Columbia, Vancouver, BC V5Z 4E3, Canada

ARTICLE INFO

Article history:
Received 30 January 2016
Revised 18 February 2016
Accepted 19 February 2016
Available online 22 February 2016

Keywords:
Triphenylphosphonium
Trifluoroborate
Fluorine-18
Myocardial perfusion imaging
Thyroid
Positron emission tomography

ABSTRACT

Four trifluoroborate derivatives of phosphonium cations **2a–d** were radiolabeled with fluorine-18 (^{18}F) and evaluated for imaging myocardial perfusion with positron emission tomography (PET). Tracers were radiolabeled simply via ^{18}F–^{19}F isotope exchange reaction in acidic (pH 2) aqueous solution. On average, [^{18}F]**2a–d** were obtained in 10–17% non-decay-corrected radiochemical yield with 25.9–48.1 GBq/μmol specific activity, and >96% radiochemical purity. In vitro stability study showed no decomposition of [^{18}F]**2a–d** after being incubated in mouse plasma for up to 2 h. Myocardial uptake in mice was visualized in PET images by using [^{18}F]**2b–d** but not [^{18}F]**2a**. [^{18}F]**2a–d** were stable against in vivo defluorination as no significant bone uptake was observed. Despite sub-optimal heart uptake of [^{18}F]**2b–d**, we successfully demonstrated that ^{18}F–^{19}F isotope exchange reaction on trifluoroborates could be a promising strategy for the design of potential ^{18}F-labeled tracers even for intracellular targets.

Nuclear imaging modalities including single photon emission computed tomography (SPECT) and positron emission tomography (PET) are used routinely in the clinic for evaluating myocardial perfusion to detect and characterize coronary artery disease.[1,2] The most widely used radiotracers for myocardial perfusion imaging are mitochondria-targeting cations ^{99m}Tc-sestamibi and ^{99m}Tc-tetrofosmin for SPECT.[2] Mitochondria are present in abundance within the myocardium, and these radiolabeled cations are drawn to the enhanced negative membrane potential of mitochondria.[2] Due to superior sensitivity and quantification capability of PET, the development of myocardial perfusion imaging agents in the past few years has focused on using positron emitters especially fluorine-18 (^{18}F) as imaging radioisotopes.[3] ^{18}F has a 109.7-min physical half-life, and can be produced in large quantity using a medical cyclotron. ^{18}F-labeled tracers can be prepared at a centralized radiopharmacy and distributed to regional hospitals for imaging. The pharmacophores commonly used for the design of ^{18}F-labeled myocardial perfusion imaging agents include phosphonium and rhodamine cations, and mitochondrial complex I inhibitors.[4–19] Among them, phosphonium has received the most attention due to the simplicity of its chemical structure.

Although several ^{18}F-labeled phosphonium cations have been reported and evaluated as potential myocardial perfusion imaging agents (Fig. 1),[4–14] most of these tracers suffer from tedious multi-step radiolabeling procedures[4,5,12,7] and/or in vivo defluorination leading to undesired high bone uptake (22.6%ID/g for [^{18}F]FMBTP at 2-h post-injection).[7,9] For example, [^{18}F]FBnTP (Fig. 1), developed by Dannals' group, is currently the most well-studied ^{18}F-labeled phosphonium cation.[20–23] However, its preparation involves four synthetic steps: ^{18}F-fluorination, reduction, bromination, and final coupling reaction with triphenylphosphine.[4] Such multi-step radiolabeling procedures could potentially limit its clinical applications due to the challenge of adapting the synthetic procedures to a commercial GMP-compliant automated synthesizer. Suitable ^{18}F-labeled phosphonium cations that are stable in vivo, and can be prepared in a single ^{18}F-fluorination step would be more appealing for routine use in the clinic.

Previously, we reported a facile strategy for the preparation of ^{18}F-labeled tracers via ^{18}F–^{19}F isotope exchange reaction using trifluoroborate derivatives.[24–27] This one-step reaction proceeds well in acidic aqueous solution (~pH 2) and obviates the lengthy drying

* Corresponding authors. Tel.: +1 604 675 8206; fax: +1 604 675 8218 (F.B.); tel.: +1 604 675 8208; fax: +1 604 675 8218 (K.-S.L.).
E-mail addresses: fbenard@bccrc.ca (F. Bénard), klin@bccrc.ca (K.-S. Lin).
† Present address: 675 West 10th Avenue, Rm 4-113, Vancouver, BC V5Z 1L3, Canada.
‡ Present address: 675 West 10th Avenue, Rm 4-123, Vancouver, BC V5Z 1L3, Canada.

http://dx.doi.org/10.1016/j.bmcl.2016.02.062
0960-894X/

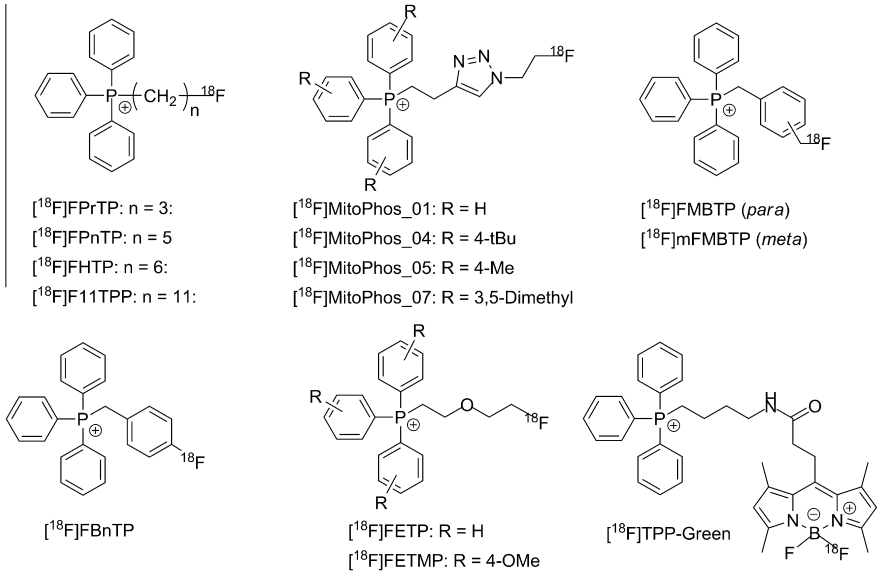

Figure 1. Structures of reported ^{18}F-labeled phosphonium cations for myocardial perfusion imaging.

step (to remove water from [^{18}F]fluoride) that is typically required for tracers prepared via aliphatic/aromatic nucleophilic substitution using [^{18}F]fluoride. Since the ^{18}F-labeled product and the radiolabeling precursor are chemically identical, in most cases, the ^{18}F-labeled trifluoroborates can be purified via solid phase extraction using a C18 Sep-Pak cartridge instead of HPLC purification. This facile radiolabeling and purification strategy can be easily implemented for clinical production using an automated synthesizer. Furthermore, we have successfully applied this strategy for the design of ^{18}F-labeled trifluoroborates targeting extracellular membrane-bound carbonic anhydrase IX,[28] integrin $\alpha_v\beta_3$,[29–31] and receptors of somatostatin,[32] bombesin,[33,34] and bradykinin.[35] None of these reported ^{18}F-labeled trifluoroborate derivatives exhibited significant bone uptake, demonstrating the stability of ^{18}F-labeled trifluoroborates against in vivo defluorination.

To exploit this radiolabeling strategy for the design of mitochondria-targeting tracers, we synthesized and compared four triphenylphosphonium bioconjugates **2a–d** (Scheme 1) that were differentially linked to an ^{18}F-labeled trifluoroborate. Instead of triphenylphosphine which was used in most ^{18}F-labeled phosphonium cations, we started with tris(4-methylphenyl)phosphine (for **2a**) or tris(3,5-dimethylphenyl)phosphine (for **2b–d**). It has been suggested that the phosphonium cations designed for heart imaging should have moderate lipophilicity (Log*P* values in the range of 0.5–1.3).[36] The extra methyl substitutions in tris(4-methylphenyl) phosphine and tris(3,5-dimethylphenyl)phosphine should provide compensation for the potential reduction in overall lipophilicity caused by the introduction of the polar dimethylammoniomethyl trifluoroborate motif. We also used different linkers between tris (3,5-dimethylphenyl)phosphine and the dimethylammoniomethyl trifluoroborate moiety in **2b** (propylene), **2c** (4,4′-bis-methylenebiphenyl) and **2d** (undecylene), so that the effect of linker selection on imaging contrast (heart-to-background) could be compared directly.

Table 1
Molecular weight, lipophilicity (Log$D_{7.4}$) and radiochemical data of [^{18}F]**2a–d**

Radiotracer	[^{18}F]**2a**	[^{18}F]**2b**	[^{18}F]**2c**	[^{18}F]**2d**
Molecular Weight (dalton)	471.4	513.4	651.6	625.6
Log$D_{7.4}$	0.11 ± 0.01 (n = 3)	1.16 ± 0.01 (n = 3)	1.90 ± 0.02 (n = 3)	2.46 ± 0.01 (n = 3)
Radiochemical Yield (%)	12 ± 4 (n = 3)	17 ± 4 (n = 3)	14 ± 4 (n = 2)	10 ± 1 (n = 2)
Radiochemical Purity (%)	98.8 ± 1.3 (n = 3)	97.2 ± 1.9 (n = 3)	96.7 ± 1.8 (n = 2)	96.7 ± 4.7 (n = 2)
Specific Activity (GBq/μmol)	40.7 ± 14.8 (n = 3)	48.1 ± 25.9 (n = 3)	25.9 ± 3.7 (n = 2)	33.3 ± 11.1 (n = 2)

The data except molecule weight are presented as mean ± SD.

The cold standards **2a–d** were prepared as depicted in Scheme 1A. First, tris(4-methylphenyl)phosphine or tris(3,5-dimethylphenyl)phosphine was reacted with excess dibromide (1,3-dibromopropane for **a** and **b**; 4,4′-bis(bromomethyl)biphenyl for **c**; 1,11-dibromoundecane for **d**) in toluene. The precipitated phosphonium bromides were filtered and reacted directly with *N*, *N*-dimethylamine to yield the intermediates **1a–d** in 13–35%

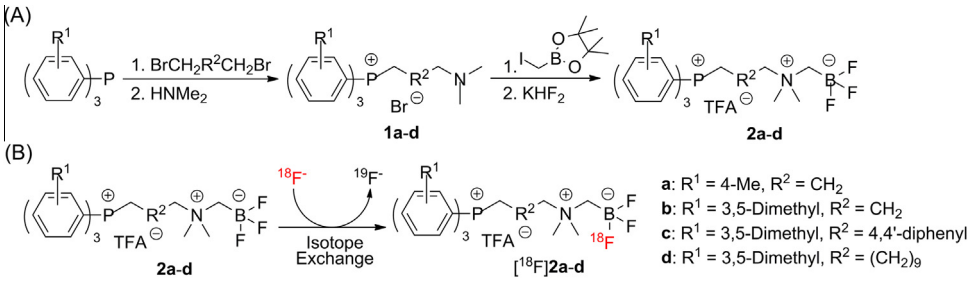

Scheme 1. Synthesis of (A) trifluoroborate derivatives of triphenylphosphonium **2a–d**, and (B) their ^{18}F-labeled analogs prepared via isotope exchange reaction.

Table 2
In vitro plasma stability of [^{18}F]**2a–d**

Radiotracers	[^{18}F]**2a**	[^{18}F]**2b**	[^{18}F]**2c**	[^{18}F]**2d**
QC	99.1	96.2	99.6	>99.9
15 min	99.0	96.2	98.2	>99.9
60 min	98.6	95.8	99.5	>99.9
120 min	99.3	96.1	98.5	>99.9

Data are presented as radiochemical purity (%) of [^{18}F]**2a–d** in QC samples, and in samples after being incubated in mouse plasma for up to 2 h

overall yield from triphenylphosphine. Compounds **1a–d** were then reacted with 2-(iodomethyl)-4,4,5,5-tetramethyl-1,3,2-dioxaborolane in dichlomethane, and the resulting quaternary ammonium iodide salts were collected as precipitates following the addition of diethyl ether. The iodides were subsequently treated with potassium hydrogen fluoride and hydrochloric acid in *N*,*N*-dimethylformamide to yield the corresponding trifluoroborates. After HPLC purification, **2a–d** trifluoroacetates were obtained in 56–69% yield from **1a–d**. The formation of trifluoroacetates was due to the addition of trifluoroacetic acid in the HPLC solvents.

Compounds **2a–d** were successfully radiolabeled with ^{18}F via ^{18}F–^{19}F isotope exchange conducted in acidic buffer (pH 2) with heating at 70 °C (Scheme 1B). [^{18}F]**2a**, [^{18}F]**2b**, [^{18}F]**2c**, and [^{18}F]**2d** were obtained in 10–17% average radiochemical yield (Table 1). Average specific activity and radiochemical purity values were 25.9–48.1 GBq/μmol and 96.7–98.8%, respectively. The lipophilicities of [^{18}F]**2a–d** were measured via the shake flask method using *n*-octanol and phosphate buffer (pH 7.4). Log$D_{7.4}$ (*D*: distribution coefficient) of [^{18}F]**2a–d** ranged from 0.11 to 2.46 (Table 1). In vitro plasma stability study was conducted, and no decomposition of [^{18}F]**2a–d** was observed after being incubated in mouse plasma at 37 °C for up to 2 h (Table 2 and Figs. S1–4). These results are in agreement with our previous reports that ^{18}F-labeled dimethylammoniomethyl trifluoroborates are stable in mouse plasma.[28,32,34,35]

To evaluate the potential of [^{18}F]**2a–d** as myocardial perfusion imaging agents, imaging/biodistribution studies were conducting using CD-1 normal mice. Representative static PET images acquired at 1-h post-injection are shown in Figure 2, while representative dynamic acquisitions showing distribution of [^{18}F]**2a–d** at earlier time points are shown in Figures S5–8. The time-activity curves of selected organs/tissues based on dynamic images are shown in Figure 3. The heart was visualized by using [^{18}F]**2b–d** but not by [^{18}F]**2a**. All tracers were excreted through both hepatobiliary and renal pathways, with a significant amount of radioactivity being retained or trapped in the renal cortex (images not shown). According to the dynamic images (Figs. S5–8), [^{18}F]**2b** exhibited the slowest initial clearance from the blood pool. Although not significant, activity in bone articulations suggests minor in vivo defluorination for each tracer.

One unexpected finding from the PET images was the relatively good uptake of [^{18}F]**2b–d** (especially [^{18}F]**2c–d**) in thyroid glands (Fig. 2). The estimated uptake of [^{18}F]**2a–d** based on the PET images were 0.28, 1.28, 2.78 and 1.58%ID/g, respectively. To the best of our knowledge, there is no formal report in literature on the thyroid uptake of radiolabeled phosphonium cations. A similar finding was recently presented as a meeting abstract.[6] Wells et al. reported 4.2 ± 2 and 17.4 ± 13 SUV (standardized uptake value) of thyroid uptake in rats at 1-h post-injection by using [^{18}F]MitoPhos_04 and [^{18}F]MitoPhos_07 (Fig. 1), respectively.[6] However, no follow-up to that work has been published. Since [^{18}F]MitoPhos_07 and [^{18}F]**2b–d** share the same tris(3,5-dimethylphenyl)phosphine motif, we believe this structure might be important for their high thyroid uptake. While the mechanism of thyroid uptake for [^{18}F]**2b–d** remains unclear at this stage, they may be useful in characterizing thyroid/parathyroid pathologies with PET. It should be noted that ^{99m}Tc-sestamibi and ^{99m}Tc-tetrofosmin have been used in conjunction with [^{99m}Tc]pertechnatate or [^{123}I]iodide to evaluate hyperparathyroidism in relation to parathyroid adenomas.[37]

The biodistribution data of [^{18}F]**2a–d** at 1-h post-injection are summarized in Table 3, and are consistent with the observations from PET images. [^{18}F]**2a** showed the lowest accumulation in intestines (9.85 ± 1.22%ID/g) but the highest accumulation in kidneys (46.0 ± 7.32%ID/g). This observation is in good agreement with the fact that [^{18}F]**2a** is more hydrophilic (Log$D_{7.4}$ = 0.11) than [^{18}F]**2b–d** (Log$D_{7.4}$ = 1.16–2.46). Although joints were visualized in PET images, the bone uptake of [^{18}F]**2a–d** was only in the range of 0.48–1.74%ID/g, confirming only minor defluorination in vivo. [^{18}F]**2a** exhibited the lowest heart uptake (0.23 ± 0.10%ID/g) such that the heart could not be visualized in PET images because of its low heart-to-muscle contrast ratio (0.88 ± 0.30). This could be due to its high hydrophilicity with a Log$D_{7.4}$ value lower than 0.5, a minimum value suggested by Zhou et al.[36] Although the heart could be clearly visualized in PET images by using [^{18}F]**2b–d**, the average heart uptake (0.76–1.37%ID/g) and contrast ratios

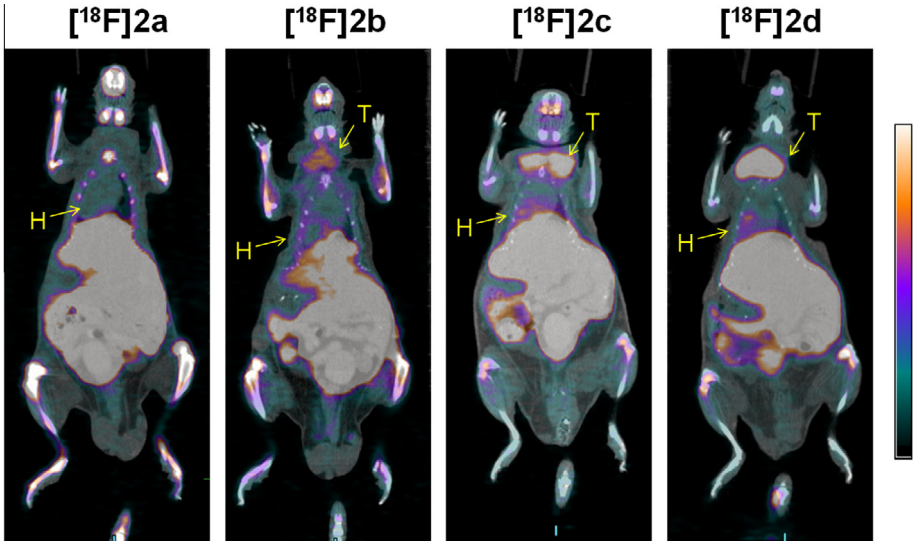

Figure 2. Static PET/CT images of ^{18}F-labeled **2a–d** in CD-1 normal mice acquired at 1-h post-injection. The scale of the color bar is 0–1.5%ID/g. H: heart; T: thyroid.

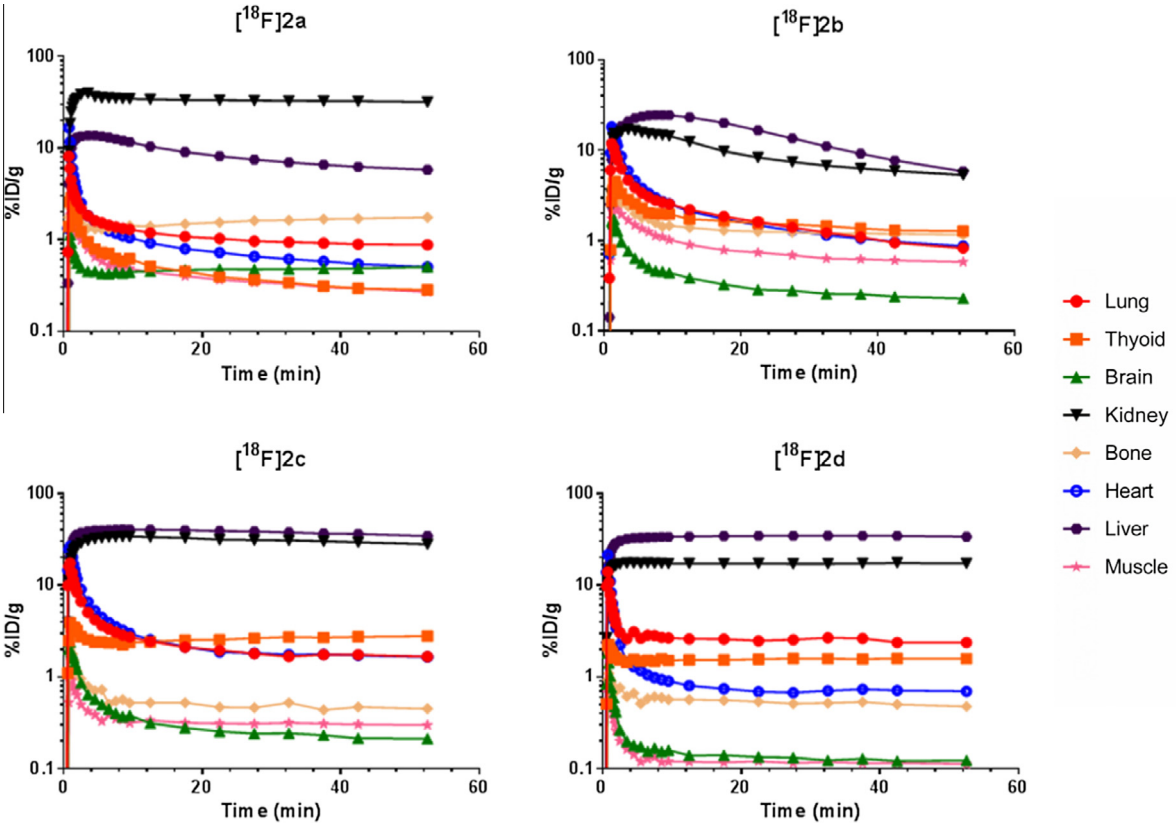

Figure 3. Time-activity curves of [^{18}F]**2a–d** in selected organs/tissues of CD-1 normal mice.

of heart-to-blood (2.06–11.8) and heart-to-muscle (1.98–6.19) were inferior to those of other reported ^{18}F-labeled phosphonium cations.[7,9,10,13,14] Since [^{18}F]**2b–d** were stable in mouse plasma, the sub-optimal heart uptake could be due to their fast blood clearance into liver and kidneys as shown in Figures 3 and S5–8. Nevertheless, our data indicate that [^{18}F]**2b–d** can cross the membrane and accumulate inside cells of interest. While a variety of ^{18}F-labeled trifluoroborates have been reported previously, those tracers were designed exclusively to image the expression of extracellular membrane-bound proteins.[28–35] The successful visualization of the heart using [^{18}F]**2b–d** suggests that ^{18}F–^{19}F isotope exchange reaction on trifluoroborates can be leveraged for the design and synthesis of ^{18}F-labeled PET tracers for imaging intracellular targets.

Table 3
Biodistribution data (%ID/g, 1-h post-injection) of [^{18}F]**2a–d** in CD-1 mice

Tissues/organs	[^{18}F]**2a** (n = 4)	[^{18}F]**2b** (n = 6)	[^{18}F]**2c** (n = 6)	[^{18}F]**2d** (n = 6)
Blood	0.11 ± 0.04	0.13 ± 0.06	0.44 ± 0.25	0.14 ± 0.12
Fat	0.02 ± 0.01	0.04 ± 0.01	0.03 ± 0.01	0.11 ± 0.09
Intestines	9.85 ± 1.22	34.4 ± 8.26	20.7 ± 5.67	19.9 ± 11.1
Stomach	0.10 ± 0.03	1.30 ± 1.53	0.23 ± 0.06	0.75 ± 0.26
Spleen	0.14 ± 0.09	0.20 ± 0.05	0.33 ± 0.05	4.93 ± 3.79
Liver	3.55 ± 1.60	2.49 ± 1.73	21.9 ± 4.67	31.4 ± 14.5
Pancreas	0.41 ± 0.10	0.44 ± 0.11	0.31 ± 0.05	2.54 ± 1.13
Kidney	46.0 ± 7.32	8.93 ± 3.74	21.8 ± 4.43	28.6 ± 17.8
Lung	0.69 ± 0.22	0.78 ± 0.47	0.37 ± 0.10	1.34 ± 0.87
Heart	0.23 ± 0.10	1.37 ± 0.42	0.76 ± 0.10	0.98 ± 0.39
Muscle	0.26 ± 0.10	0.74 ± 0.30	0.21 ± 0.02	0.16 ± 0.06
Bone	1.74 ± 0.36	1.24 ± 0.40	0.48 ± 0.15	1.44 ± 0.66
Brain	0.02 ± 0.01	0.04 ± 0.02	0.03 ± 0.01	0.05 ± 0.04
Heart/blood	2.24 ± 0.97	11.8 ± 4.45	2.06 ± 0.88	10.5 ± 6.77
Heart/muscle	0.88 ± 0.30	1.98 ± 0.50	3.62 ± 0.42	6.19 ± 1.34

In conclusion, we have successful synthesized four ^{18}F-labeled trifluoroborate derivatives of phosphonium cations **2a–d**, and evaluated their potential as myocardial perfusion imaging agents. These ^{18}F-labeled trifluoroborates were prepared in one-step using an ^{18}F–^{19}F isotope exchange reaction, and showed no significant defluorination in vivo. Despite visualization of the heart, heart uptake and heart-to-background contrasts of [^{18}F]**2b–d** were inferior to most of reported ^{18}F-labeled phosphonium cations. The unexpected uptake of [^{18}F]**2b–d** in thyroid warrants further investigation, and understanding the mechanism for the uptake of [^{18}F]**2b–d** into thyroid might one day lead to a better management of thyroid diseases.

Acknowledgements

This work was supported by the Canadian Institutes of Health Research (MOP-126121) and the BC Leading Edge Endowment Fund. The authors would like to thank Milan Vuckovic, Wade English, and Julius Klug for operating the cyclotron, and Nadine Colpo and Navjit Hundal-Jabal for assisting the imaging studies.

Supplementary data

Supplementary data associated with this article can be found, in the online version, at http://dx.doi.org/10.1016/j.bmcl.2016.02.062.

References and notes

1. Travin, M. I. *Semin. Nucl. Med.* **2015**, *45*, 392.
2. Sogbein, O. O.; Pelletier-Galarneau, M.; Schindler, T. H.; Wei, L.; Wells, R. G.; Ruddy, T. D. *BioMed Res. Int.* **2014** 942960.
3. Brunken, R. C. *J. Nucl. Med.* **2015**, *56*, 1478.
4. Ravert, H. T.; Madar, I.; Dannals, R. F. *J. Label. Compd. Radiopharm.* **2004**, *47*, 469.

5. Haslop, A.; Wells, L.; Gee, A.; Plisson, C.; Long, N. *Mol. Pharm.* **2014**, *11*, 3818.
6. Wells, L.; Haslop, A.; Coello, C.; Keat, N.; Gee, A.; Passchier, J.; Long, N.; Plisson, C. *J. Nucl. Med.* **2014**, *55*, 121.
7. Zhao, Z.; Yu, Q.; Mou, T.; Liu, C.; Yang, W.; Fang, W.; Peng, C.; Lu, J.; Liu, Y.; Zhang, X. *Mol. Pharm.* **2014**, *11*, 3823.
8. Li, L.; Brichard, L.; Larsen, L.; Menon, D. K.; Smith, R. A. J.; Murphy, M. P.; Aigbirhio, F. I. *J. Label. Compd. Radiopharm.* **2013**, *56*, 717.
9. Kim, D.-Y.; Kim, H.-J.; Yu, K.-H.; Min, J.-J. *Nucl. Med. Biol.* **2012**, *39*, 1093.
10. Kim, D.-Y.; Kim, H.-J.; Yu, K.-H.; Min, J.-J. *Bioorg. Med. Chem. Lett.* **2012**, *22*, 319.
11. Yuan, H.; Cho, H.; Chen, H. H.; Panagia, M.; Sosnovik, D. E.; Josephson, L. *Chem. Commun.* **2013**, 10361.
12. Haslop, A.; Gee, A.; Plisson, C.; Long, N. *J. Label. Compd. Radiopharm.* **2013**, *56*, 313.
13. Kim, D.-Y.; Kim, H.-J.; Yu, K.-H.; Min, J.-J. *Bioconjugate Chem.* **2012**, *23*, 431.
14. Kim, D.-Y.; Kim, H.-S.; Le, U. N.; Jiang, S. N.; Kim, H.-J.; Lee, K.-C.; Woo, S.-K.; Chung, J.; Kim, H.-S.; Bom, H.-S.; Yu, K.-H.; Min, J.-J. *J. Nucl. Med.* **2012**, *53*, 1779.
15. Gottumukkala, V.; Heinrich, T. K.; Baker, A.; Dunning, P.; Fahey, F. H.; Treves, S. T.; Packard, A. B. *Nucl. Med. Biol.* **2010**, *37*, 365.
16. Bartholomä, M. D.; Gottumukkala, V.; Zhang, S.; Baker, A.; Dunning, P.; Fahey, F. H.; Treves, S. T.; Packard, A. B. *J. Med. Chem.* **2012**, *55*, 11004.
17. Bartholomä, M. D.; He, H.; Pacak, C. A.; Dunning, P.; Fahey, F. H.; McGowan, F. X.; Cowan, D. B.; Treves, S. T.; Packard, A. B. *Nucl. Med. Biol.* **2013**, *40*, 1043.
18. Yalamanchili, P.; Wexler, E.; Hayes, M.; Yu, M.; Bozek, J.; Kagan, M.; Radeke, H. S.; Azure, M.; Purohit, A.; Casebier, D. S.; Robinson, S. P. *J. Nucl. Cardiol.* **2007**, *14*, 782.
19. Tsukada, H.; Nishiyama, S.; Fukumoto, D.; Kanazawa, M.; Harada, N. *J. Nucl. Med.* **2014**, *55*, 473.
20. Madar, I.; Huang, Y.; Ravert, H.; Dalrymple, S. L.; Davidson, N. E.; Isaacs, J. T.; Dannals, R. F.; Frost, J. J. *J. Nucl. Med.* **2009**, *50*, 774.
21. Higuchi, T.; Fukushima, K.; Rischpler, C.; Isoda, T.; Javadi, M. S.; Ravert, H.; Holt, D. P.; Dannals, R. F.; Madar, I.; Bengel, F. M. *J. Nucl. Med.* **2011**, *52*, 965.
22. Madar, I.; Ravert, H.; DiPaula, A.; Du, Y.; Dannals, R. F.; Becker, L. *J. Nucl. Med.* **2007**, *48*, 1021.
23. Madar, I.; Ravert, H. T.; Du, Y.; Hilton, J.; Volokh, L.; Dannals, R. F.; Frost, J. J.; Hare, J. M. *J. Nucl. Med.* **2006**, *47*, 1359.
24. Liu, Z.; Pourghiasian, M.; Radtke, M. A.; Lau, J.; Pan, J.; Dias, G. M.; Yapp, D.; Lin, K.-S.; Benard, F.; Schaffer, P.; Perrin, D. M. *Angew. Chem., Int. Ed.* **2014**, *53*, 11876.
25. Liu, Z.; Li, Y.; Lozada, J.; Lin, K.-S.; Schaffer, P.; Perrin, D. M. *J. Label. Compd. Radiopharm.* **2012**, *55*, 491.
26. Liu, Z.; Lin, K.-S.; Benard, F.; Pourghiasian, M.; Kiesewetter, D. O.; Perrin, D. M.; Chen, X. *Nat. Protoc.* **2015**, *10*, 1423.
27. Liu, Z.; Hundal, N.; Wong, M.; Yapp, D.; Lin, K.-S.; Benard, F.; Perrin, D. M. *MedChemComm* **2014**, *5*, 171.
28. Lau, J.; Liu, Z.; Lin, K.-S.; Pan, J.; Zhang, Z.; Vullo, D.; Supuran, C. T.; Perrin, D. M.; Benard, F. *J. Nucl. Med.* **2015**, *56*, 1434.
29. Liu, Z.; Radtke, M.; Wong, M.; Lin, K.-S.; Yapp, D.; Perrin, D. M. *Bioconjugate Chem.* **2014**, *25*, 1951.
30. Liu, Z.; Li, Y.; Lozada, J.; Wong, M. Q.; Greene, J.; Lin, K.-S.; Yapp, D.; Perrin, D. M. *Nucl. Med. Biol.* **2013**, *40*, 841.
31. Li, Y.; Liu, Z.; Wong, M. Q.; Lin, K.-S.; Yapp, D.; Perrin, D. M. *Nucl. Med. Biol.* **2013**, *40*, 959.
32. Liu, Z.; Pourghiasian, M.; Benard, F.; Pan, J.; Lin, K.-S.; Perrin, D. M. *J. Nucl. Med.* **2014**, *55*, 1499.
33. Li, Y.; Liu, Z.; Harwig, C. W.; Pourghiasian, M.; Lau, J.; Lin, K.-S.; Schaffer, P.; Benard, F.; Perrin, D. M. *Am. J. Nucl. Med. Mol. Imaging* **2013**, *3*, 57.
34. Pourghiasian, M.; Liu, Z.; Pan, J.; Colpo, N.; Lin, K.-S.; Perrin, D. M.; Benard, F. *Bioorg. Med. Chem.* **2015**, *23*, 1500.
35. Liu, Z.; Amouroux, G.; Zhang, Z.; Pan, J.; Hundal-Jabal, N.; Colpo, N.; Perrin, D. M.; Benard, F.; Lin, K.-S. *Mol. Pharm.* **2015**, *12*, 974.
36. Zhou, Y.; Liu, S. *Bioconjugate Chem.* **2011**, *22*, 1459.
37. Smith, J. R.; Oates, M. E. *Radiographics* **2004**, *24*, 1101.